

Neutron Resonance Spin Echo

Wolfgang Besenböck, Peter Hank, Maro Köppe, Roland Gähler,
 †Thomas Keller, †Robert Golub

Fakultät für Physik, Technische Universität München, D-85747 Garching, Germany
 †Hahn-Meitner-Institut, Glienicker Str. 100, D-14109 Berlin, Germany

(Received 1 February 1996; accepted 2 July 1996)

RF-flipper coils open various possibilities in neutron physics: spin echo spectrometers, small angle scattering instruments, new types of interferometers, and applications in particle optics. We want to explain the basic principles of the coils and their applications.

KEYWORDS: Neutron spin echo, Polarized neutrons, Neutron optics, Neutron scattering

1. Introduction

We suppose that next century's neutron guide halls will look more like optical laboratories than like machine halls - there is no dramatic increase of primary source intensity within sight, but new frontiers might be opened by future high precision instrumentation. Some of these new instruments will probably be based on high frequency magnetic flipper coils. These coils can coherently split neutron beams in space and/or time; they can simulate magnetic fields of very high precision and stability; and they can be used for time-of-flight applications with resolutions around 100 ns.

The following explanations will be based on quantum mechanics, because for combinations of several flipper coils it is tedious to follow the classical movement of the neutron magnetic moment μ_n . Describing a neutron in a magnetic field B as a two-level system, with transitions induced by the RF-field, is more convenient and more instructive. On the other hand, most instruments are easier to describe in a classical way, and we will follow this whenever it is appropriate. Quantum-mechanical and classical descriptions, of course, give the same result, as long as the potential energy $\mu_n B$ of the neutron in the field is small compared to its total energy, which should always be true here.

2. The flipper coils

For the following applications it is necessary to split neutrons coherently in two beams with different k -vectors. Such a splitting can comfortably be achieved by flipper coils consisting of an RF-field B_R rotating with Larmor-frequency ω_L in the xy -plane and a static field $B_Z = \omega_L/\gamma_n$ in z -direction (see fig 1). Neutrons, traveling in y -direction and polarized in x -direction, are split at the boundary of the static field in two states Ψ^+ and Ψ^- with different polarization relative to the field B_Z . The magnetic interaction leads to a change in kinetic energy from E_0 to $E_0 \pm \mu_n \cdot B_Z$. The RF-field is matched in amplitude and frequency ($\omega_L = 2\Delta\omega$) to invert completely the population of both states, causing an exchange in total (and potential) energy of $\Delta E = 2\hbar\Delta\omega = \mp 2\mu_n \cdot B_Z$, but — since there is no field gradient — no change in the kinetic energy. At the second field boundary, the potential energy is again converted to kinetic energy. After passage through one flipper coil we have two beams with different kinetic and

total energy (in each case $\pm \mu_n \cdot B_Z$), leading to beats in space and time between both states. A detailed quantummechanical calculation of a flipper coil is given in ref. 1. Calculations for comparable systems can be found for example in ref. 2-4.

The change in kinetic energy also causes a splitting of the k -vector by $\Delta k = \pm 2\mu_n \cdot B_Z/\hbar v$ where v is the n -velocity. The splitting in k by a flipper coil with static field strength B_Z is equal to the splitting at the boundary of a static field of the strength $2 \cdot B_Z$, which can easily be deduced from fig. 1.

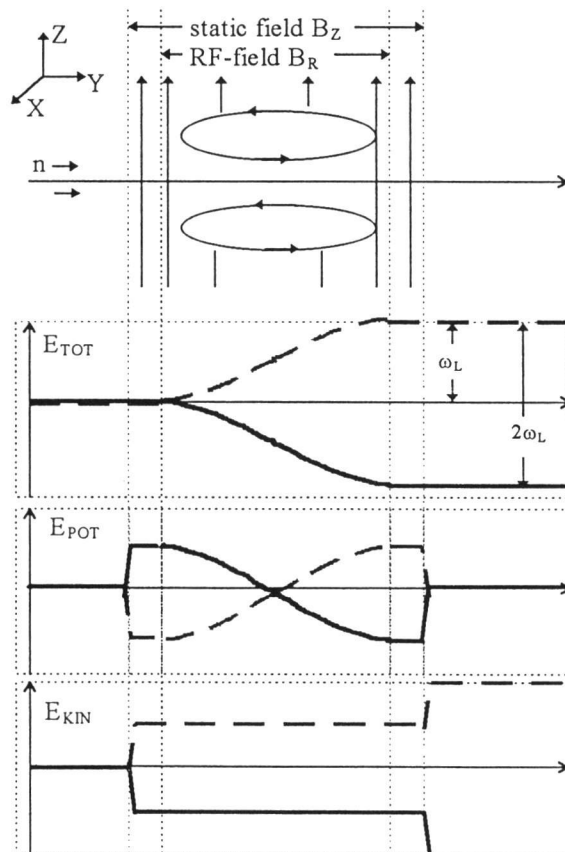


Fig.1. The changes in total, potential and kinetic energy for a neutron in a flipper-coil.

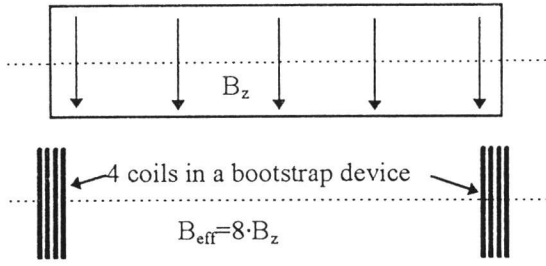


Fig.2. A bootstrap device with 4 coils (N coils) can simulate a static magnetic field of effective strength $B_{\text{EFF}} = 8 \cdot B_z$ ($B_{\text{EFF}} = 2 \cdot N \cdot B_z$).

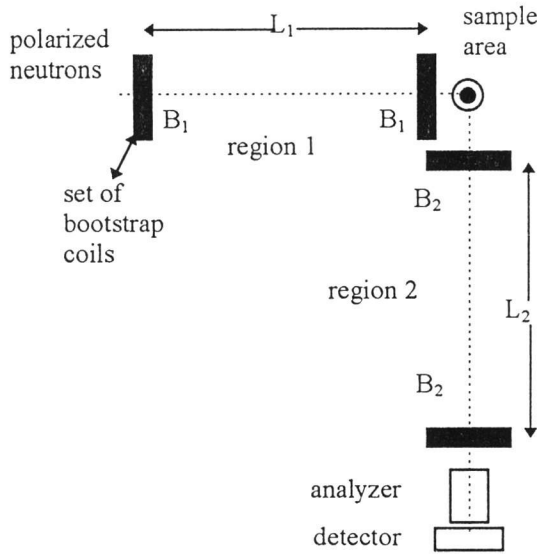


Fig.3. Principle structure of a spin echo spectrometer

3. Magnetic pseudo fields

We will now show that RF-flippers can be used to simulate magnetic fields. The effect from magnetic fields on the wave function of a neutron can be written in matrix notation $\Psi = \hat{O}\Psi_0$ with $\Psi_0 = (\Psi^+ | \Psi^-)$. In the case of a static magnetic field B_z , \hat{O} can be written as

$$\hat{O}_B = \begin{pmatrix} e^{-i\Delta k y} & 0 \\ 0 & e^{i\Delta k y} \end{pmatrix}, \quad \Delta k = k_0 \frac{\mu_n B_z}{2E_0}, \quad (1)$$

whereas for the flipper coil from above, \hat{O} becomes

$$\hat{O}_{\text{RF}} = \begin{pmatrix} 0 & -i \\ -i & 0 \end{pmatrix} \begin{pmatrix} e^{i2\Delta\alpha x} & 0 \\ 0 & e^{-i2\Delta\alpha x} \end{pmatrix} \begin{pmatrix} e^{-i2\Delta k y} & 0 \\ 0 & e^{i2\Delta k y} \end{pmatrix},$$

$$\Delta k = k_0 \frac{\mu_n B_z}{2E_0}. \quad (2)$$

The first factor of \hat{O}_{RF} is just the spinflip. The second factor gives rise to oscillations (beats) in time, i. e., to a rotation of the spin direction as a function of time, whereas the third factor gives oscillations in space (Larmor-precession). By multiplying the matrices from eq.2, we see that for $\Delta\omega \cdot t = \Delta k \cdot y$, i.e. $t = 1/v \cdot y$, there will be no oscillations. This is due to the trivial fact that an observer

moving with the neutrons (velocity v) in a field-free region does not see any beats, i.e. no spin precession.

For two RF-flippers with static fields B_z separated by a distance L , the wave function directly behind the flippers will be the same as the wave function behind a magnetic field with length L and strength $2 \cdot B_z$ (the time dependent factors and the spin flip cancel):

$$\Psi = \begin{pmatrix} e^{-i2\Delta k L} & 0 \\ 0 & e^{i2\Delta k L} \end{pmatrix} \Psi_0. \quad (3)$$

This corresponds to a classical precession angle of $\varphi = 2\Delta k \cdot L$. Because eq.3 and eq.1 are the same (for $y=L$), the assembly of two flipper coils separated by L , can be regarded as a 'pseudo field' (see fig.2). Because Δk depends on the RF-frequency rather than on B_z , pseudo fields can be extremely stable.

To simulate even higher static fields, one can replace the single flipper coils by stacks of two or more flipper coils with alternating B_z fields ('bootstrap method'). Due to this reversal from one flipper to the next within the first stack, the states Ψ^+ and Ψ^- always exchange their roles, and by each coil, the splitting in k and ω will be enhanced by $2\Delta k$ and $2\omega_L$. In the second stack of coils, the splitting is reduced step by step back to zero. The operator for a pseudofield made of two stacks of N flipper coils will be:

$$\hat{O}_{\text{NRF}} = (\hat{O}_{\text{RF}})^N = \begin{pmatrix} e^{-iN\Delta k y} & 0 \\ 0 & e^{iN\Delta k y} \end{pmatrix}, \quad (4)$$

$$\Delta k = N \cdot k_0 \frac{\mu_n B_z}{E_0}.$$

4. Neutron resonance spin echo spectrometer NRSE

The NRSE-spectrometer^{6,7)} is like a spin echo spectrometer,^{8,9)} where each precession field is replaced by flipper coils (or bootstrap-coils) (see fig.3). At present we mostly use bootstrap coils with $N=2$. In this case B_{EFF} is four times the static field strength B_z .

The classical angle of polarization φ is given by the phase difference between the two states. The phase difference at the last coil in front of the analyzer results from the integral of Δk over the pathlength in the field or pseudo field, with opposite fields in region 1 and 2:

$$\varphi = 2\Delta k_1 \cdot L_1 - 2\Delta k_2 \cdot L_2 = \frac{\Delta E_1 \cdot L_1}{v_1} - \frac{\Delta E_2 \cdot L_2}{v_2} \quad (5)$$

$$= \gamma \left(\frac{B_{\text{EFF}1} \cdot L_1}{v_1} - \frac{B_{\text{EFF}2} \cdot L_2}{v_2} \right).$$

The indices refer to the first (second) field region. We see that φ will be independent of the incident velocity for $v_1 = v_2$ when the spin echo condition $B_1 \cdot L_1 = B_2 \cdot L_2$ is fulfilled. For small energy changes, $\hbar\omega$, during sample scattering, we get to first order in ω ⁵⁾:

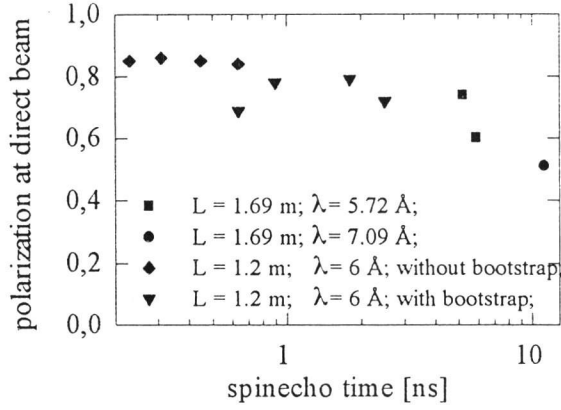


Fig. 4. Resolution curve of the NRSE-spectrometer at Saclay. Recently the spin echo time range was extended down to <10 ps by means of an additional set of low-field NSE-coils.

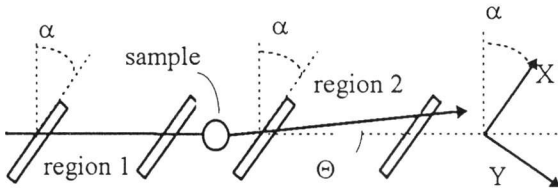
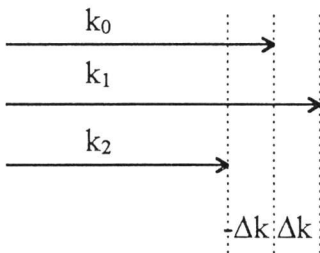
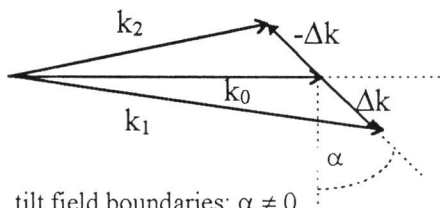


Fig.5. Scheme of a NRSE-spectrometer with tilted coils for small angle scattering. All flipper coils are tilt by an angle α with respect to the beam. Regions 1 and 2 are the two pseudo fields.



field boundaries normal to beam axis: $\alpha = 0$



tilt field boundaries: $\alpha \neq 0$

Fig.6. The k -splitting with tilt magnetic field boundaries.

$$\begin{aligned} \varphi &= \frac{\gamma \cdot B_{EFF1} \cdot L_1}{v_1} - \frac{\hbar \gamma \cdot B_{EFF2} \cdot L_2}{v_1} \left(1 - \frac{\omega}{2E} \right) \\ &= \frac{\gamma \cdot B_{EFF1} \cdot L_1}{m v_1^3} \cdot \omega = \tau \cdot \omega, \end{aligned} \quad (6)$$

where τ is called spin echo time and is a measure for the resolution of the spectrometer. If we associate wave packets with each spin state, we get a simple interpretation

of τ : it is the difference in travel time for the two packets being split by $2\Delta k_1$ over the length L_1 . The same holds for L_2 and Δk_2 . This splitting of a wavepacket — in contrast to a spreading in a standard TOF-spectrometer — is the reason, why $S(q, t)$, the intermediate scattering function, and not $S(q, \omega)$ is measured in spin echo (to be published).

5. Tilt coils

A NSE- or NRSE-spectrometer with tilt magnetic field or pseudo field boundaries (fig.5) may be used for measurements of phonon lifetimes¹⁰⁾ and for high resolution elastic small-angle scattering.¹¹⁾

The splitting $\pm \Delta k$ is perpendicular to the field boundaries (fig.6). In the tilted coordinate system of fig.5, only the k_y components of the neutrons will be split, and the effective field length is given by its y -component. For small angle scattering by Θ , we have to consider in eq.5 variations of φ with Θ (to first order) in addition to variations of φ with Δv :

$$\begin{aligned} \varphi &= \frac{\gamma \cdot B_1 L_1 \cdot \cos(\alpha)}{v_1 \cdot \cos(\alpha)} - \frac{\gamma \cdot B_2 L_2 \cdot \cos(\alpha)}{(v_1 + \Delta v) \cdot \cos(\alpha + \Theta)} \quad (7) \\ &\cong \tau \cdot \omega + \kappa \cdot \Theta \end{aligned}$$

$$\kappa = \frac{\gamma \cdot B_{EFF1} L_1}{v_1} \cdot \tan(\alpha);$$

One can see that a small variation in scattering angle is transformed to a large variation in the angle of polarization φ , as κ can be very big ($\kappa \leq 10^5$). For elastic small angle scattering ($\omega = 0$), the setup shares some properties with a double crystal spectrometer (DCS), made out of perfect crystals, as the beam divergence can be orders of magnitude bigger than the measurable deflection. In contrast to DCS, long wavelengths may be used here, and hence higher resolution is possible. In a quantum mechanical picture, κ/k_0 is just the lateral splitting of the two states at the sample, and so κ/k_0 (for the maximum κ) is a measure of the maximum width of inhomogeneities measurable in a small angle scattering experiment.

From eq.7 we see that we obtain also an echo for

$$d\omega/d\theta = -\kappa/\tau; \quad (\varphi = \text{const.}) \quad (8)$$

as long as ω can be taken as proportional to Θ within the Θ acceptance of the spectrometer. Eq.8 is the basis for measurements of phonon linewidths, where the instrumental parameters κ and τ are matched to the slope of the dispersion curve $\omega(\Theta)$ or $\omega(q)$, where q is the momentum transfer. Actually this picture is too simple: the echo condition eq.5 looks different for inelastic scattering; the acceptable wavelength band is narrower than for quasielastic scattering; and the angle α is different for both pseudo fields. For details see ref. 6, 7, 11.

In real experiments, the condition $d\omega/d\theta = \text{const.}$ is often violated and quadratic corrections have to be taken into account. We want to note without proof that by additional pseudo fields, with different angles α , these quadratic corrections are possible.

Tilt coils can also be applied to increase the angular acceptance of NRSE-spectrometers by replacing each

non-tilt field by two tilt ones. Errors in φ from beam divergence can be corrected up to second order.

6. Mieke-spectrometer

The fourth coil of a complete NRSE-spectrometer is placed exactly at the echo-position. At this coil the ω -splitting is brought back to zero, leading to a stationary final state — the measured phase angle is not time dependent and can be detected anywhere downstream of the last flipper coil. If the frequency ω_2 of that coil is changed to any other value, say ω_D , the echo-condition is still fulfilled at this position, but the final state becomes time dependent, i.e., it will be modulated by $2(\omega_2 - \omega_D)$.

Three cases are of special interest:

a. $|\omega_D - \omega_2| \leq 10$ Hz. In this case the signal gets modulated with frequencies of several Hertz and can be analyzed by standard lock-in techniques. Small signals sitting on a high and time varying background can be detected in this way (fig. 8a).

b. $\omega_D = 0$, i.e. the fourth coil is omitted. In this case we get beats of frequency $4\omega_2$ at the echo-point. Like in NRSE the observability of this echo is restricted to an area l_E around the echo-point (given by $\Delta k \cdot l_E \cdot d\lambda/\lambda \cong 2\pi$), where $d\lambda/\lambda$ is the width of the incoming wavelength band (typically 0.1). In practice l_E can be down to ≤ 1 mm — too small to place analyzer and detector there. Actually the analyzer can be put anywhere between the third coil and the echo-point: in this region there is no spin precession, consequently the echo point is not influenced by the analyzer's position⁵⁾. Of course in this case it needs near the echo-point a detector with very high time resolution and very small active thickness (≈ 0.1 mm), because $4\omega_2$ is in the MHz-region (fig. 7b). A measured signal from a MIEZE2-setup is given in fig. 9.

c. A variant of MIEZE2 is possible by combining the second and the third coil to one with frequency ω_2 . In this case the echo condition is changed to

$$\omega_1 L_1 = (\omega_2 - \omega_1) L_2 \quad (9)$$

which can be deduced from fig. 8c.

Now the scattering sample has to be placed in a region of high k -splitting, and consequently variations ΔL in path length due to sample scattering have to be kept small compared to $1/\Delta k$, otherwise serious phase deterioration occurs. This limits its application to small angle scattering — in practice angles $\theta \leq 5^\circ$ are possible. On the other hand this effect may be used to measure long range correlations in a sample (chapter 8).

A MIEZE1 or MIEZE2 spectrometer with very high energy resolution could be implemented in existing SANS-instruments; it does not need large area analyzers-downstream of the sample. Large area detectors with the required time resolution are available¹²⁾.

The MIEZE1-setup might find applications in parity violation experiments in nuclear reactions with polarized neutrons¹³⁾, where correlations between the direction of emitted γ 's and the polarization of absorbed neutrons are examined. If we omit the analyzer in MIEZE1, the spin arrives at the echo-point with spin direction given by

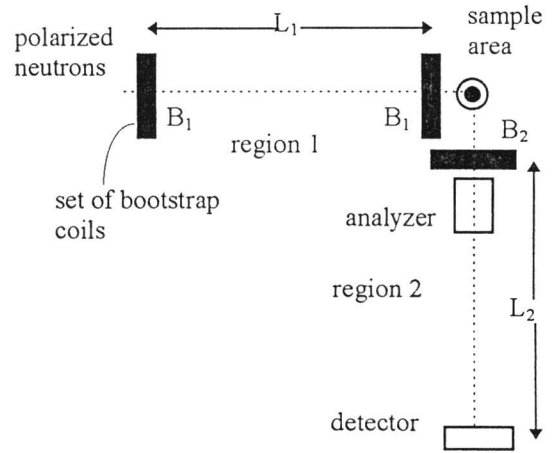


Fig.7. Principle structure of a MIEZE-spectrometer

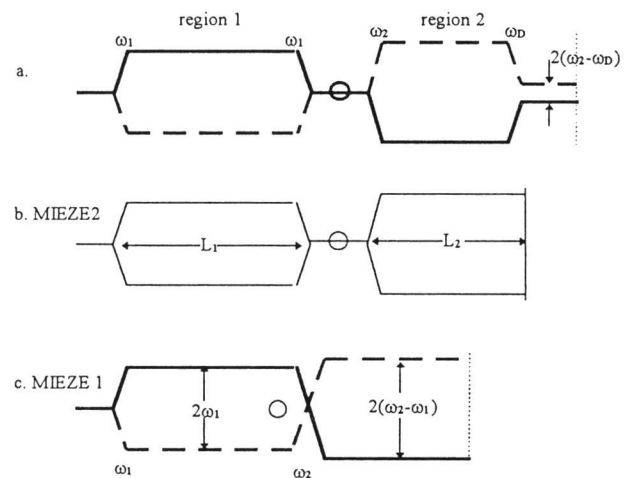


Fig.8. Level schemes of the various versions of MIEZE spectrometers. For $\omega_D = \omega_2$, (a) gives the level scheme of the NRSE spectrometer. The circles are the sample positions and the dotted lines are the detector positions. The echo condition can easily be transformed into a condition that the enclosed areas between both states have to be the same for region 1 and 2.

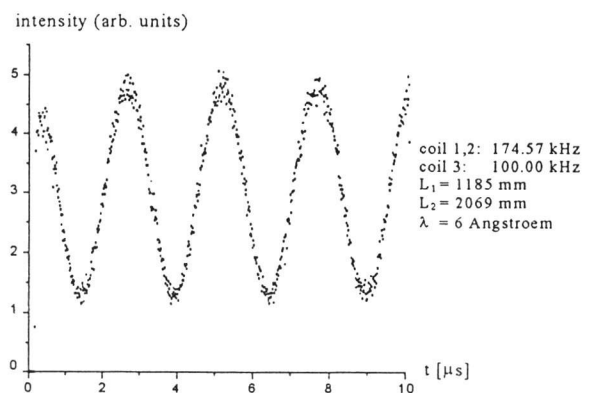


Fig.9. TOF spectrum from a MIEZE2 setup.

$\varphi = 4(\omega_2 - \omega_1) \cdot t$, and within the γ -detectors the same frequency can be sensed by correlation techniques. Note that this frequency can be varied in a very wide range and that (for a polychromatic n-beam) the signal is limited to a close region around the n-absorber (given by the width of the echo curve). There is a strong reduction of correlated

background, because there is no neutron polarization outside of this area.

In fig. 9 we show the measured time signal for a MIEZE2-setup. Because of the bootstrap-coils, the signal frequency (400 kHz) is four times the RF-frequency of the third coil (100 kHz). Resetting of the time occurs always after 10^{-5} s, i.e., the pattern shows 4 full periods of oscillations.

7. Comparison MIEZE - MZI

In the following we show that a MIEZE-spectrometer is the time analogue of a spatial Mach-Zehnder-interferometer (MZI), based on sine phase gratings.

We assume (see fig.10) for the MZI appropriate phase gratings with lattice constants a_ν ($\nu = 1,2$) and with corresponding lattice constants $G_\nu = 2\pi/a_\nu$. To first order the angular splitting will be $\alpha = G_1/k_0$ and $\beta = (G_2 - G_1)/k_0$, and from geometry we see that $G_1 \cdot L_1 = (G_2 - G_1) \cdot L_2$ holds.

This equation is similar to the basic MIEZE-equation (eq. 9). The MZI "spatial frequencies" G_ν correspond to the "time frequencies" ω_ν from MIEZE. The longitudinal splitting of the matter wave frequencies ($\omega_0 \pm \omega_\nu$) in the MIEZE case corresponds to a lateral k -splitting in the MZI case. It is this analogy that justifies for MIEZE the name "Mach-Zehnder in time". MIEZE is somehow a more efficient interferometer than a MZI relying on gratings, because intensity losses due to diffraction into wrong orders (states) cannot be avoided, whereas in MIEZE there are only two possible states (spin = $\pm 1/2$).

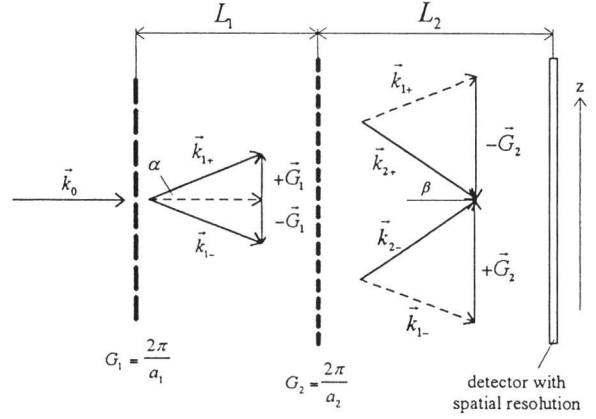
We now assume a scattering sample near the plane of the second grating (second coil). In case of the MZI, coherent waves emitted from distant parts (distance d) of the sample (due to the lateral separation between both beams) are superposed at the detector and the contrast of the MZI pattern is sensitive to phase shifts resulting from density variations within length scales $\leq d$. In case of MIEZE, waves emitted at two different times (separated by τ_{MIEZE}), are superposed at the detector. τ_{MIEZE} is given by the difference Δt in flight time for wavepackets with two wavevectors $k_0 \pm \Delta k$ traveling from the first to the second coil. Thus the contrast of the MIEZE-intensity pattern is sensitive to phase shifts from temporal changes of the local density of the sample with time scales comparable or smaller than τ_{MIEZE} . Consequently a MIEZE-spectrometer can be used for quasielastic n-scattering experiments.

Tilting the coils (like in fig.5) leads to lateral and longitudinal beam splitting, and a MIEZE setup is now an interferometer in space and time, giving beats in space and time at the detector. This can be regarded as a "sideband interferometer", first introduced in ref. 14. A similar interferometer based on moving gratings was proposed in ref. 15.

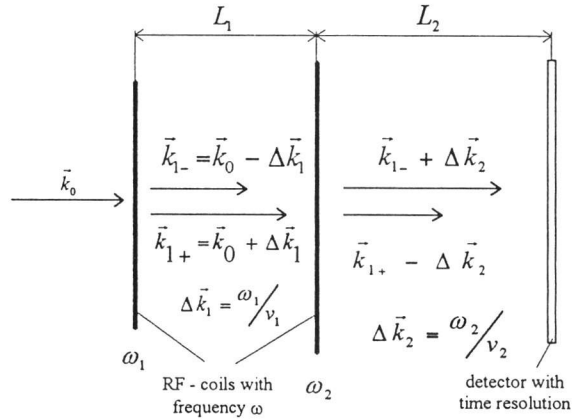
8. Neutron Spin Optics (NSO)

Standard neutron optics is severely hindered by the extremely low source brilliance for slow neutrons and the rather small neutron wavelength. These difficulties can be circumvented in several cases, if, not the wavelength itself, but the "beat wavelength" between the amplitudes from two

Mach Zehnder interferometer (MZI):



MIEZE spectrometer:



Intensity pattern at the detector

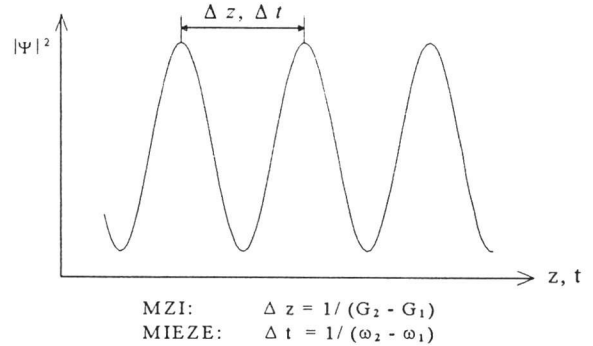


Fig.10. Comparison of a Mach-Zehnder interferometer (MZI) with a MIEZE spectrometer. In the MZI, the lateral k -splitting leads to the well known spatial interference pattern. For MIEZE, the splitting is longitudinal, i.e., in $|k|$ and consequently in ω , and at the detector we get beats in time.

states with slightly different k -vectors, is directly used as wavelength in optical experiments. This method is possible with perfect crystal optics¹⁶⁾ and also with static magnetic fields or pseudo fields, which will be explained here.

For convenience we will assume now real magnetic fields and use the classical spin-description (Larmor precession). Larmor precession shares two basic properties with matter waves, traveling in free space:

a) The phase φ_L of the Larmor precession is proportional to the pathlength, the neutron travels inside the field B (assumed to fill the whole space). The same holds for the

phase of the matter wave and λ_L , the beat wavelength between both states, corresponds to the matter wavelength.

b) The expectation value of the polarisation $\langle\sigma\rangle$ is a linear superposition of the magnetic moments from all particles arriving at one point. The same holds for matter waves, where the field amplitude $\langle\Psi\rangle$ is given by a linear superposition of all waves arriving at one point.

Typical values for $\lambda_L = 2\pi v/\gamma B$ range from μm to cm . The properties a and b are sufficient to create diffraction effects, thus we reproduce optical effects with very large effective wavelengths by measuring $\langle\sigma\rangle$.

There are certain differences between particle optics and spin optics, which might be best explained in an example — n-diffraction from a double slit (fig.11).

a) In NSO we have free access to the phase of the incoming wave, as we can control the polarization at the input slit S_1 . This can be used to demonstrate and study coherence effects.

b) Within each slit, neutron intensity has to be scattered fairly isotropic, avoiding spin flip scattering. In this case, the Huygens-principle is fulfilled and the diffraction pattern appears.

c) The dispersion is different in NSO: $\lambda_{\text{NSO}} \sim v$ holds, whereas in particle optics $\lambda \sim 1/v$ is valid, and NSO does not obey the standard Schrödinger equation.

d) In the plane of observation, the amplitude and phase of $\langle\sigma\rangle$ is determined by a measurement of σ_x and σ_y using a polarizer in front of the detector. The measured signal does not correspond to the intensity but to the amplitude of the pattern. To first order, neutron intensity will be constant within the whole region of the diffraction pattern, points with zero intensity in ordinary optics just correspond to zero polarization.

e) In order to avoid the need of highly monochromatic neutrons in NSO, the resonance spin echo principle should be used. If the echo condition is fulfilled in the plane of observation, there will be no dephasing due to the velocity dependence of λ_{NSO} and a broad velocity band ($\Delta v/v \approx 10\%$) can be applied.

It is worth noting that in the above example we can reproduce the double slit pattern without assuming each neutron to pass both slits. We want to apply NSO to rather sophisticated wave optical phenomena like the phase anomaly near focus¹⁷⁾ or the Anderson localization¹⁸⁾. There should be also applications in neutron diffraction, where NSO offers a possibility to measure long range correlations (above μm length scale), for example in high strength compound materials.

In NSO, the amplitude $\langle\sigma\rangle$ is built up by individual magnetic moments from many independent particles and there is no need of any coherence of the real matter waves. The authors are not aware if NSO might lead to a model for an elementary particle consisting of a large number of individual carrier particles.

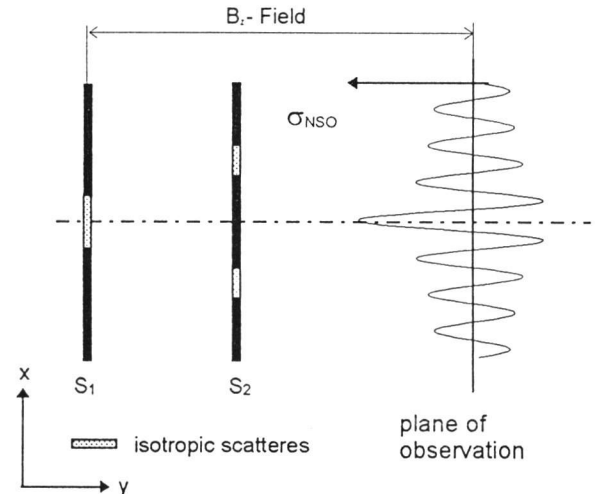


Fig.11. The NSO double slit experiment. Neutrons polarized in x direction enter from the left. Within slit S_1 and the double slit S_2 neutrons are isotropically scattered. In the plane of observation, σ_{NSO} is measured in x and y direction with help of polarizers. The normal double slit pattern is obtained by calculating $|\sigma_{\text{NSO}}|^2$.

- 1) R. Golub, R. Gähler, T. Keller: *Am. J. Phys.* 62 (1994) 779
- 2) Badurek G., Rauch H., Zeilinger A.: in Ref.9, S.136
- 3) Weihrauch W., Krüger E., Nistler W.: in Ref.9, S.94
- 4) Shirley J.H.: *Phys.Rev.*138 (1965) B979
- 5) P.Hank: *Aufbau und Test eines höchstauflösenden Neutronenspektrometers auf Basis von Spinflippern*, diploma thesis TU München, E21 (1995)
- 6) R. Golub, R. Gähler: *Phys. Lett. A* 123 (1987) 43
- 7) T. Keller: *Höchstauflösende Neutronenspektrometer auf der Basis von Spinflippern-neue Varianten des Spin Echo Prinzips*, diss. TU München (1993)
- 8) F. Mezei: *Z. Phys.* 255 (1972) 146
- 9) F. Mezei: *Neutron spin echo, Lecture notes in physics*, Vol. 128, Springer Berlin (1980)
- 10) F. Mezei: in *Neutron inelastic scattering 1977, IAEA, Vienna* (1978) 125 and: T. Keller, R. Gähler, H. Kunze, R. Golub: *Neutron news*, vol. 2. nr. 3 (1995)
- 11) R. Pynn, in Ref.6 159
- 12) V. Dangendorf et al, *NIMA*350 (1994) 503
- 13) P.A. Krupchitsky: *NIMA*284 (1989) 71
- 14) R. Golub, S.K. Lamoreaux: *Phys. Lett. A* 162 (1992) 122
- 15) A.I. Frank, V.G. Nosov: *Phys. Atomic Nuclei*57 (1994) 968
- 16) K. Raum: *Gravitations- und Inertialeffekte in der Neutronenoptik*, diss. Innsbruck, Feb.96
- 17) M. Born, E. Wolf; *Principles of Optics*, Oxford: Pergamon, 6.ed. 1981
- 18) P.W. Anderson: *Phys.Rev.* 109 (1958) 1492